Taylor & Francis
Taylor & Francis Group

Journal of Macromolecular Science, Part A
Pure and Applied Chemistry

ISSN: 1060-1325 (Print) 1520-5738 (Online) Journal homepage: www.tandfonline.com/journals/lmsa20

Bone-targeted stimuli-responsive polymeric nanocarriers for osteosarcoma treatment

Isinsu Mutlu, Tugba Gencoglu-Katmerlikaya, Sezen Atasoy & Aydan Dag

To cite this article: Isinsu Mutlu, Tugba Gencoglu-Katmerlikaya, Sezen Atasoy & Aydan Dag (2025) Bone-targeted stimuli-responsive polymeric nanocarriers for osteosarcoma treatment, Journal of Macromolecular Science, Part A, 62:12, 1238-1250, DOI: 10.1080/10601325.2025.2571964

To link to this article: https://doi.org/10.1080/10601325.2025.2571964

JOURNAL OF MACROMOLECULAR SCIENCE, PART A: PURE AND APPLIED CHEMISTRY
2025, VOL. 62, NO. 12, 1238–1250
https://doi.org/10.1080/10601325.2025.2571964

Bone-targeted stimuli-responsive polymeric nanocarriers for osteosarcoma treatment

Isinsu Mutlu[a], Tugba Gencoglu-Katmerlikaya[a], Sezen Atasoy[b], and Aydan Dag[c,d]

[a]Department of Biotechnology, Institute of Health Sciences, Bezmialem Vakif University, Istanbul, Turkey; [b]Department of Biochemistry, Faculty of Pharmacy, Bezmialem Vakif University, Istanbul, Turkey; [c]Department of Pharmaceutical Chemistry, Faculty of Pharmacy, Bezmialem Vakif University, Istanbul, Turkey; [d]Pharmaceutical Application and Research Center, Bezmialem Vakif University, Istanbul, Turkey

ABSTRACT

Osteosarcoma, a highly aggressive bone tumor commonly diagnosed in adolescence, has major treatment challenges due to metastasis and chemoresistance. This study presents the development of bone-targeted, pH-sensitive polymeric dual drug delivery systems based on a triblock copolymer, P(BPMA-b-OEGMEMA-b-FPMA), synthesized *via* reversible addition-fragmentation chain transfer (RAFT) polymerization. After deprotection of the BPMA segments, the chemotherapeutic agent doxorubicin (Dox) and/or the bone-targeting drug alendronate (Aln) were loaded onto the polymer, resulting in self-assembled nanomicelles. Dynamic light scattering (DLS) analysis showed that the hydrodynamic diameters of the Dox-loaded (M1), Aln-loaded (M2), and dual drug-loaded (M3) micelles were approximately 100.00 ± 6.34 nm, 97.70 ± 4.39 nm, and 89.86 ± 4.77 nm, respectively, with narrow size distributions. *In vitro* cytotoxicity assays demonstrated that the dual-loaded micelles (M3) exhibited significantly higher selective toxicity against SAOS-2 osteosarcoma cells compared to free drugs, while maintaining low toxicity toward healthy HUVEC endothelial cells. Cellular uptake studies confirmed enhanced internalization of the bone-targeted nanocarriers by SAOS-2 cells. These findings highlight the potential of this novel polymeric system to improve therapeutic outcomes by effectively targeting bone tumor cells and minimizing side effects through controlled and selective drug delivery.

GRAPHICAL ABSTRACT

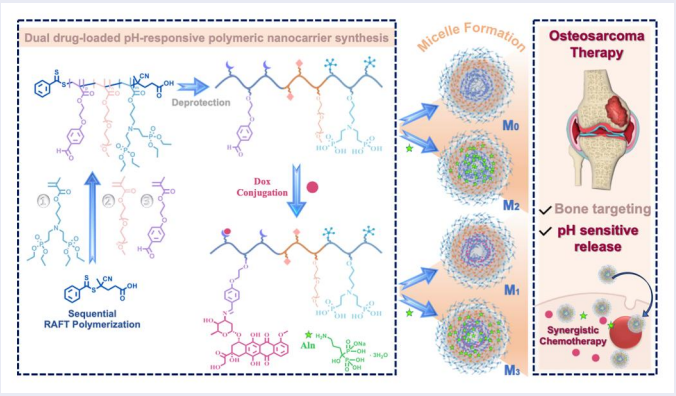

ARTICLE HISTORY
Received August 2025
Accepted October 2025

KEYWORDS
Alendronate; doxorubicin; dual drug delivery; osteosarcoma; bone-targeted; pH sensitive

1. Introduction

Osteosarcoma (OS) is a primary malignant tumor of the bone that occurs in children and the elderly, with a slightly higher incidence in men.[1] Increasing survival rates has been challenging as OS is an aggressive cancer with unknown molecular pathways of both etiology and pathophysiology. The prevailing therapeutic modality constitutes a multifaceted, multidisciplinary regime encompassing radiotherapy, chemotherapy, surgical intervention, and subsequent adjuvant chemotherapy. Treatment strategies mostly involve surgical removal of the tumor at some point, supported by adjuvant or neoadjuvant chemotherapy.[2] Currently, with limited chemotherapy, the long-term survival rate for a newly diagnosed resectable OS patient is 60-70%, which has remained largely unchanged over the past decades. The chemotherapy regimens include various combinations of doxorubicin (Dox), high-dose methotrexate, cisplatin, and ifosfamide.[3,4] However, these treatments have severe side effects because most of the drugs have only a limited selectivity for malignant tissue.

CONTACT Aydan Dag aydandag@gmail.com Department of Pharmaceutical Chemistry, Faculty of Pharmacy and Pharmaceutical Application and Research Center, Bezmialem Vakif University, 34093 Istanbul, Turkey.

Supplemental data for this article can be accessed online at https://doi.org/10.1080/10601325.2025.2571964.

Consequently, the primary goal of OS therapy is currently to treat malignant cells specifically without damaging healthy tissue. Alendronate sodium is a member of the bisphosphonate class of drugs, which have an inhibitory effect on bone resorption by osteoclasts. It binds to the surface of the bone and has a high affinity for the hydroxyapatite (HA) crystals of the bone matrix. It is mainly used in the pharmacotherapy of bone diseases such as osteoporosis, Paget's disease, and bone cancer, making it a potential bone-targeting molecule.[5,6] A unique treatment for OS is represented by the coupling of the chemotherapeutic agents with targeting ligands, whereby the aforementioned challenges can be overcome by active targeting.

Bone-targeted drug delivery systems are designed to achieve better drug distribution than conventional pharmacotherapy, which faces bone tissue barriers such as poor permeability and bone remodeling that limit local drug accumulation.[7,8] In recent years, the controlled delivery of therapeutics to bone tissue with specific bone-targeting ligands has attracted increasing attention for the treatment of bone-related diseases as an effective strategy to improve efficacy with reduced side effects. Ligands such as bisphosphonates, oligopeptides, and aptamers have been conjugated to the surface of drug-loaded nanomedicines, resulting in improved targeting.[9–14] Among various bone-targeting ligands, bisphosphonates are promising materials compared to small molecules and peptides, mainly due to the ease of large-scale preparation and the high molecular weight property to serve as independent drug carriers.[15–18] In controlled drug delivery systems, the use of polymers is particularly advantageous. Synthetic polymer structures are generally preferred and they are more useful than biological polymers because of the design of the carrier system and the availability of modifications to its physicochemical properties. Synthetic polymeric drug delivery systems (PDDS) can be designed to be activated in the target tissue, have long term stability in the blood circulation, have low toxicity and immunogenicity and protect drugs from degradation. In a PDDS, the active molecule can be entrapped in the polymer, encapsulated in it or simply conjugated to it. Stimuli-responsive PDDS are often preferred because they can provide controlled drug release at the desired site, time, and concentration. Acidic environments (pH 6.5–7.2), which are known to be specific for the tumor microenvironment, or enhanced enzymatic activations are used to ensure target-specific release of the carrier system, especially when designing for the tumor region. For this reason, many pH-sensitive DDS structures have been designed to have covalent bonds between the drug and polymeric backbone which degrade under acidic conditions.[19–21] Investigations for bone-targeting PDDS have demonstrated that polymer composition plays a critical role in enhancing bone affinity, primarily through multiple secondary interactions with bone tissue components, including inorganic minerals, organic matrix proteins, and resident cells. Drawing from these insights, we hypothesized that incorporating polybisphosphonate segments into the polymer backbone could facilitate a range of such interactions within the complex bone microenvironment, thereby improving targeting efficiency and therapeutic efficacy.

Taking advantage of bond cleavage under mildly acidic conditions, pH-responsive amphiphilic polymeric micelles serve as effective drug delivery systems by promoting targeted drug release within the tumor microenvironment, thereby enhancing accumulation at the disease site and minimizing systemic side effects. In this study, we report the successful synthesis of pH-responsive polymeric micelles functionalized either through covalent immobilization of Dox or encapsulation of alendronate (Aln). Their *in vitro* therapeutic efficacy was systematically evaluated against OS cell lines, demonstrating promising potential for targeted cancer therapy. The amphiphilic triblock copolymer P(BPMA-b-OEGMEMA-b-FPMA) was successfully synthesized *via* reversible addition–fragmentation chain transfer (RAFT) polymerization. The incorporation of 3-(bis(2-(diethylphosphoryl)ethyl)amino)-propyl methacrylate (BPMA) units into the copolymer backbone provided a platform for the development of targeted DDS with enhanced tumor localization through dual synergistic therapy. Moreover, the incorporation of POEGMEMA units into the polymer chain increases the biocompatibility and prolongs blood circulation time of drugs. Following the successful synthesis, the triblock copolymer was loaded with Dox, Aln or both, resulting in self-assembled nanostructures categorized as mono-drug-loaded micelles—M_1 (Dox only) and M_2 (Aln only)—and dual-drug-loaded micelles, M_3 (Dox + Aln). Comprehensive characterization of these nanocarriers included evaluation of their drug release profiles, bone-targeting capabilities, and physicochemical properties. Finally, *in vitro* assays were conducted to assess their therapeutic efficacy against OS.

2. Materials and methods

All precursor molecule synthesis and nuclear magnetic resonance (NMR) characterization were given in the supporting material (SI).

2.1. Synthesis of polymers

2.1.1. Synthesis of poly(3-(bis(2-(diethylphosphoryl)ethyl)amino)propyl methacrylate homopolymer via RAFT polymerization (P(BPMA), P1)

3-(Bis(2-(diethylphosphoryl)ethyl)amino)propyl methacrylate (BPMA) (0.73 g, 1.55 mmol) was placed in a small vial and dissolved in 2.20 mL of toluene. 4-cyano-4-(phenylcarbonothioylthio)pentanoic acid (CPADB, 9.20 mg, 0.31 mmol) and the initiator azobisisobutyronitrile (AIBN, 0.50 mg, 3.09 μmol) were then added to the vial, which was quickly closed. The reaction mixture was purged with nitrogen for 30 min at 0 °C to remove oxygen, followed by polymerization at 70 °C for 14.5 h. The reaction was quenched by immersing the vial in an ice bath for 5 min and subsequently exposing the system to air. The reaction mixture was evaporated using a rotary evaporator, dissolved in tetrahydrofuran and then precipitated twice in diethyl ether. Homopolymer was dried in a vacuum oven overnight. The

products were characterized by gel permeation chromatography (GPC) and proton NMR (^{1}H-NMR) spectroscopy.[22]

2.1.2. Synthesis of P(BPMA-b-OEGMEMA) diblock copolymer via RAFT polymerization (P2)

P(BPMA) homopolymer (0.3 g, 27.03 µmol, $M_{n,NMR}$= 11.10 kDa) as a macro-RAFT agent was taken into a small vial and dissolved with 1.92 mL of toluene. Poly(oligo(ethylene glycol) methacrylate) (POEGMEMA) (M_n = 300) (0.97 g, 3.24 mmol) and AIBN (0.55 mg, 3.38 µmol) were added to the vial, which was then quickly closed. The reaction mixture was degassed by purging with nitrogen for 30 min at 0 °C. Polymerization was then conducted at 70 °C for 8 h. The reaction was quenched by immersing the vial in an ice bath for 5 min, followed by exposure to air. The resulting mixture was subsequently precipitated twice into cold diethyl ether to purify the polymer. It was dried in a vacuum oven overnight. The products were characterized by GPC and ^{1}H-NMR spectroscopy.[23]

2.1.3. Synthesis of P(BPMA-b-OEGMEMA-b-FPMA) triblock polymer (P3)

P(BPMA-*b*-OEGMEMA) diblock copolymer (0.3 g, 7.30 µmol, $M_{n,NMR}$= 41.10 kDa) as a macro-RAFT agent was taken into a small vial and dissolved with 1.64 mL of toluene. 2-(4-Formylphenoxy)ethyl methacrylate (FPMA, 0.205 g, 0.88 mmol) and AIBN (0.18 mg, 1.09 µmol) were added to the vial, which was then quickly closed. The reaction mixture was purged with nitrogen for 40 min at 0 °C. The polymerization was carried out in bulk at 70 °C for 6 h. The reaction was terminated by placing the vial into an ice bath for 5 min and introducing air. The mixture was precipitated twice in cold diethyl ether. It was dried in a vacuum oven overnight. The products were characterized by GPC and ^{1}H-NMR spectroscopy.[24]

2.1.4. Deprotection of P(BPMA-b-OEGMEMA-b- FPMA) triblock polymer (P4)

For hydrolysis of triblock P(BPMA-*b*-OEGMEMA-*b*-FPMA) copolymer (0.10 g, 1.53 µmol, $M_{n,NMR}$= 65.20 kDa) was added in a flame dried, round bottom flask with a stir bar and dissolved with 10 mL anhydrous dichloromethane. Trimethylsilyl chloride (TMSCl, 2.5 mL, 0.19 mmol) was slowly added to the flask and the reaction took place at room temperature for 15 h. After that,methanol was added to the flask to terminate the reaction process and the reaction mixture was stirred for 20 h at room temperature. At the end of the 20 h solvent was evaporated in a rotary evaporator, the polymer was dissolved with THF and precipitated to diethyl ether. The copolymer was filtered and dried under a vacuum oven overnight. The products were characterized by GPC and ^{1}H-NMR spectroscopy.[25]

2.1.5. Synthesis of polymeric micelles

The dissolution of the triblock copolymer (10 mg, 0.16 µmol, $M_{n,NMR}$= 61.50 kDa) in DMSO (1 mL) was followed by the addition of Dox hydrochloride (30 eq) in the presence of triethylamine (30 eq). The vial was wrapped in aluminum foil and left to mix overnight. The drug-loaded polymer was first dialyzed against water to remove the DMSO and unconjugated drug and then lyophilized. The Dox conjugation efficiency was determined using ^{1}H-NMR. To obtain a Dox-loaded micellar structure (M1), the Dox-loaded triblock copolymer (5 mg) was dissolved in DMSO (1 mL) and added dropwise using a syringe pump at 20-second intervals for 15 min to ultra-pure water (4 mL), achieving a final concentration of 1 mg/mL. Dialysis was performed quickly to remove the DMSO. The empty micelles (M0) were prepared in a similar way using the P(BPMA-*b*-OEGMEMA-*b*-FPMA)-hyd (P4) polymer. To prepare Aln-loaded micelles, Aln (4 mg) was mixed with either 5 mg of P4 (M2) or P4-Dox (M3) in DMSO (1 mL), and the same procedure was followed. The Dox loaded samples were measured in UV–vis spectrophotometer directly after harvesting, Aln-loaded samples were treated with ferric chloride in perchloric acid solution before UV-vis measurement according to reference literature.[26] The drug loading efficiency and capacity for Aln was determined using UV–vis analysis. Drug loading capacity (LC) and encapsulation efficiency (EE) were calculated based on established methods reported in the literature.[22] Moreover, micelle formulations were characterized by dynamic light scattering (DLS) and transmission electron microscopy (TEM).

2.1.6. Drug release

Drug release rate experiment was performed in two different pH buffer solutions (pH = 5.5 and pH = 7.4). Dox only (M1) or dual drug-loaded micelles (M3) were placed into dialysis bags (MWCO 3.5 kDa). Micelles were dialyzed against 15 mL of phosphate-buffered saline (PBS) in the thermo-controlled shaker with a stirring speed of 120 rpm at 37 °C. At predetermined time points, including 1, 2, 4, 6, 10, 24, 36, 48, 56, 72, and 80 h, the amount of Dox released from either M1 or M3 was measured using UV-vis absorbance at 500 nm. The following relationships were used to calculate the cumulative drug release: At represents the amount of drug released from either M1 or M3 at time t, and A_0 represents the amount of drug loaded into M1 or M3.[24]

2.1.7. Critical micelle concentration (CMC)

DLS analysis was used to determine the CMC values of M3. Briefly, 15 different concentrations of micellar solution were prepared, ranging from 800 to 0.8 µg/mL. Measurements were repeated 5 times to ensure reproducibility. For each sample, correlation functions and photon counts per second (derived count rate, expressed in kcps) were collected without accounting for laser power attenuation. These values were plotted against concentrations, and the intersection of the two lines formed by these values gave the CMC.[27]

2.1.8. Micelle stability in serum

Serum stability of the dual drug-loaded micelle M3 was evaluated using a one-week stability assay, with particle size

monitored by DLS as described in Liu et al.[28] Initially, the micelles were prepared freshly in distilled water at a concentration of 1 mg/mL. An equal volume of DMEM containing 10% FBS was then added to the micelle solution, resulting in a final micelle concentration of 0.5 mg/mL. The mixture was then divided into two separate vials, one of which was incubated in a 37 °C orbital shaker and the other stored at 4 °C. Particle size measurements were performed at regular intervals over a period of seven days to assess micelle stability under both conditions.

2.1.9. Bone binding assay

Bone targeting properties of protected polymeric micelle, M_1 and M_3 were estimated by a HA binding assay *in vitro* while comparing the effect of BPMA backbone of polymer and Aln agent using the Dox as a fluorescence marker. Dox-loaded P3 polymer was used as a positive control. Micelles were used with equal quantities (7.6 mg/mL) of Dox content. Then samples with powdered HA (63 mg) as a representation of bone matrix were vortexed for 5 min and then incubated, with 3 mL of PBS (pH 7.4) at 37 °C in a 15 mL falcon tube. Control groups were also prepared with the same conditions except the presence of HA powder. Then, the incubated samples were centrifuged for 5 min and supernatant (1 mL) was harvested after 0, 5, 15, 30, 45 and 60 min, respectively. Unbound Dox loaded micelles were detected using a UV-vis spectrometer in the range between 495 and 505 nm wavelengths. The degree of HA binding, expressed as percent binding, was determined as the mean of three independent experiments using the following formula: [(Dox-loaded micelles concentration without HA)-(Dox-loaded micelles concentration with HA)]/(Dox-loaded micelles concentration without HA)x 100%.[29]

2.2. In vitro assays

2.2.1. Cell viability assay

To determine the cytotoxicity of the nanocarriers, (3-(4,5-dimethylthiazol-2-yl)-2,5-diphenyltetrazolium bromide (MTT) assay was performed with 10 different concentrations (100-0.2 μg/mL) for M_0, M_1, M_2, M_3, free Dox and free Aln on human endothelial cell line (HUVEC) and human OS cell line (SAOS-2). Briefly, 5×10^3 cells/well were seeded into a 96-well plate with a growth medium. After overnight incubation, the cells were treated with increasing doses of samples for 24 h. At the end of the time point, 10 μL of MTT solution was added into the wells. After 3 h incubation, the medium was discarded, 100 μL of DMSO was added and A_{540} values were recorded using a microplate reader. All the experiments were carried out in triplicates, and the results were presented as mean ± standard deviation (SD).[22,30] The half-maximal inhibitory concentration (IC_{50}) values were calculated using non-linear regression analysis in GraphPad Prism version 10 (GraphPad Software, USA) based on cell viability data obtained from MTT assay.[31]

2.2.2. Cellular internalization assay

Fluorescence microscopy was used to evaluate the intracellular uptake properties of nanocarriers in HUVEC and SAOS-2 cells. Briefly, 2×10^5 cells were seeded into a 12-well plate with the growth medium. After allowing cells overnight incubation for adhering, cells were treated with 20 μg/mL M1, M3 (samples contains 0.44 μg/mL Dox and M3 contains 1.1 μg/mL Aln) and 0.44 μg/mL free Dox for 6 and 12 h. Cells treated with only growth media were used as a control. At the end of time points, growth medium, including samples was discarded, cells were washed with 1X PBS and stained with diamidino-2-phenylindole (DAPI) for visualization of cell nuclei. The total fluorescence intensity calculation was described in previous studies.[32,33]

2.2.3. Scratch assay

Scratch assay was performed to evaluate the migratory capacity of HUVEC and SAOS-2 cells after free Dox, M1 and M3 treatments with equal doses used in cellular internalization assay. For this purpose, cells were seeded into 24 well plates and incubated at 37 °C and 5% CO_2. Once cells were confluent, a sterile 200 μL pipette tip was used to make a straight scratch and wells were washed with PBS. Low serum medium containing samples were added into each well and imaged at 0 h taken immediately using an inverted microscope. After incubating for 6 h and 12 h, images were taken at the time points and wound closure was quantified by measuring the scratch area for each time point using ImageJ software, as previously reported.[34]

2.2.4. Statistical analysis

Statistical analyses and data visualization were conducted using GraphPad Prism (v10.5.0). One-way ANOVA with Tukey's post-hoc test was applied for multiple group comparisons, while Student's t-test was used for two-group analyses. Results are expressed as mean ± standard deviation (SD), with statistical significance defined as $^{*}p < 0.05$, $^{**}p < 0.01$, $^{***}p < 0.001$, $^{****}p < 0.0001$.

3. Results and discussion

This study presents a design for an amphiphilic polymeric nanocarrier system that is co-loaded with Dox and Aln for use in dual drug delivery applications targeting OS (Scheme 1). A series of precursor compounds were first synthesized to construct the amphiphilic triblock copolymer (see SI, Figures S1 and S2). The triblock copolymer was then prepared *via* a three-step, sequential, RAFT polymerization process. Initially, the CPADB RAFT agent was employed to synthesize a PBPMA homopolymer, which subsequently served as a macro-RAFT agent for the polymerization of the hydrophilic POEGMEMA block, followed by the incorporation of the functional FPMA block. This well-controlled polymerization strategy enabled the precise architecture and functionality that are essential for efficient dual drug loading and targeted delivery.

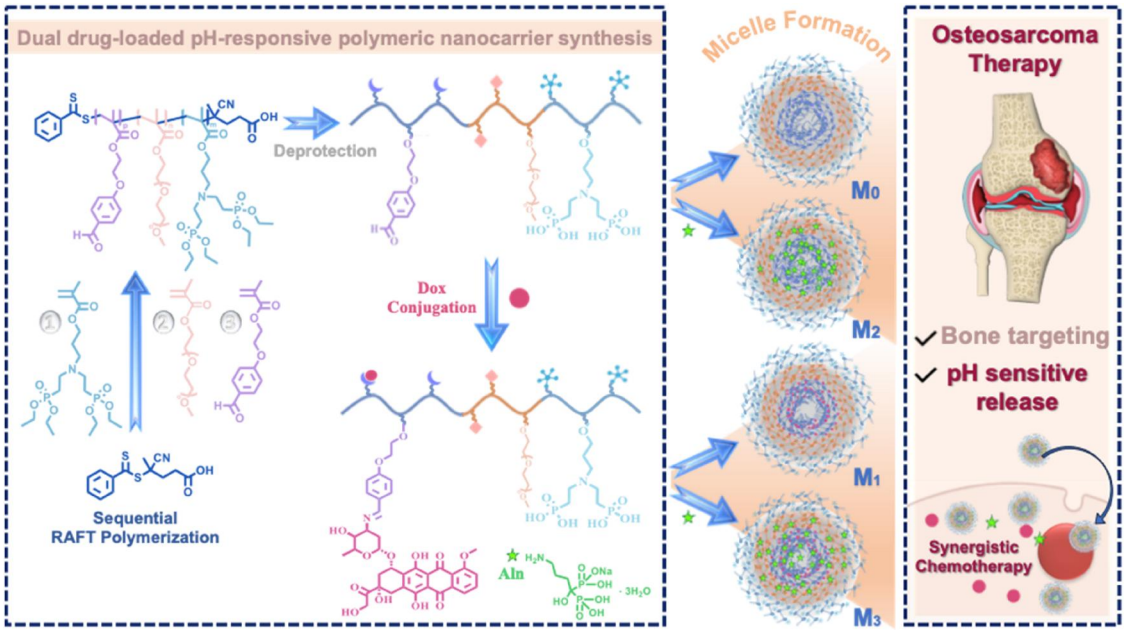

Scheme 1. Preparation of dual drug-loaded polymeric nanocarrier with bone-targeting capability and schematic diagram of its synergistic therapeutic effect on osteosarcoma.

A summary of all polymerization steps and corresponding characterization methods is provided in Table 1. GPC analysis was performed to confirm the successful incorporation of each monomer and to reflect changes in composition with increasing molecular weight. GPC analyses were conducted in tetrahydrofuran (THF) for P1 and P2, and in dimethylformamide (DMF) for P3 and P4. The results indicated that all polymers exhibited monomodal molecular weight distributions with low polydispersity indices ($Đ < 1.3$), suggesting well-controlled polymerizations and uniform chain growth.

The molecular weight and composition of the amphiphilic triblock P(BPMA-*b*-OEGMEMA-*b*-FPMA) polymer and its precursor polymers were also determined by ^{1}H-NMR. Figure 1(a) shows the ^{1}H-NMR spectrum of the P(BPMA) homopolymer. The characteristic peaks at 4.17–3.87 ppm (signals a and d), 2.78 ppm (signal c), and 2.49 ppm (signal b) are attributed to the –O–CH_2 and –NCH_2– protons of the BPMA backbone. The degree of polymerization (DP) of P(BPMA) was calculated to be 23, based on the integration ratio of the RAFT agent's terminal phenyl protons (ph) to the backbone protons (a and d). This result was further corroborated by the integration ratio of the –NCH_2– protons (b and c), which are associated with the BPMA units. DP of the POEGMEMA block in the diblock copolymer was calculated by comparing the integration of the –NCH_2– protons (signals b and c) from the BPMA segment with the integration of the –OCH_3 protons (signal f) of the OEGMEMA segment, yielding a DP value of 100. The DP of the PFPMA block in the triblock copolymer was determined by comparing the integration of the BPMA backbone protons (signals b and c) with that of the –COH proton (signal h) and the aromatic ring protons of the FPMA segment. Based on these integration ratios, the DP of the FPMA block was calculated to be 103.

The triblock copolymer was subjected to hydrolysis using trimethylsilyl chloride (TMSCl) and methanol to selectively remove the ethyl protecting groups from the bis(diethylphosphonate) moieties of the BPMA units, thereby generating bisphosphonic acid functionalities along the polymer backbone. The success of the deprotection reaction was confirmed by both ^{1}H-NMR spectroscopy and FTIR spectroscopy. As shown in Figure 1(a), ^{1}H-NMR analysis revealed quantitative removal of the ethyl groups, as evidenced by the disappearance of characteristic signals corresponding to the methyl (1.34 ppm) and methylene (4.09 ppm) protons of the bis(diethylphosphonate) groups. Importantly, this transformation occurred without cleavage of the ester linkages between the polymer backbone and the pendant groups, indicating that the hydrolysis was highly selective and did not compromise the structural integrity of the polymer. Furthermore, the reduced intensity of the aforementioned peaks relative to the resonances at 3.60 ppm (OEGMEMA), 6.96 ppm (FPMA aromatic protons), and 2.64 ppm (–NCH_2– protons, signal c) further supported the complete and efficient deprotection of the phosphonate esters with minimal loss of functional side groups or polymer degradation.

Following the controlled synthesis and hydrolysis of the triblock copolymer, Dox was covalently conjugated *via* the formation of an imine bond between the aldehyde group of the FPMA units and the primary amine of Dox. Successful conjugation was confirmed by ^{1}H NMR spectroscopy, as evidenced by the appearance of distinct peaks corresponding to the aromatic –OH protons of Dox at 14.05 and 13.25 ppm, alongside a notable decrease in the intensity of the aldehyde proton signal (i) of FPMA at 9.74 ppm (Figure 1(b)). The degree of Dox conjugation was quantitatively assessed by comparing the integral values of the four –NCH_2– protons (c) from the BPMA repeating units at 2.64 ppm with the two aromatic protons (g) from the FPMA units at 6.98 ppm. The reduction in the aldehyde proton

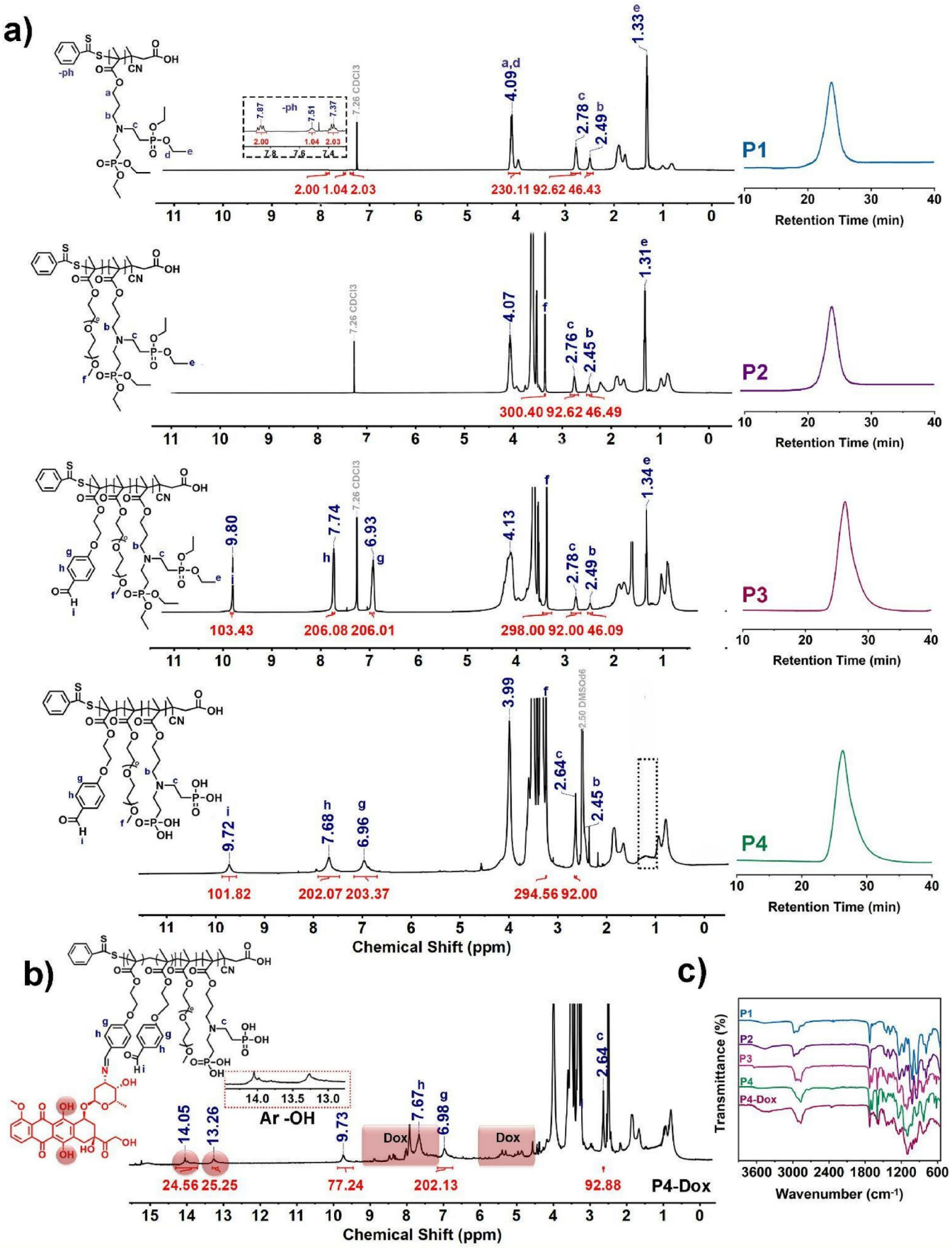

Figure 1. a) ^{1}H-NMR spectra and GPC chromatograms of P1-P4 polymers, b) ^{1}H NMR spectrum of P4 polymer after Dox loading (P4-Dox), c) FTIR spectra of P1-P4 polymers.

resonance at 9.74 ppm and the emergence of the Dox –OH signals at 13.26 and 14.05 ppm confirmed the formation of the imine linkage. Based on integration analysis, approximately 25 Dox molecules were conjugated to the triblock copolymer chain. Drug conjugation was carried out by loading a maximum of 30 units of Dox onto the triblock polymer, and Dox conjugation efficiency was 83.3% according to these results.

The FTIR spectra presented in Figure 1(c) exhibited characteristic absorption bands and incorporation of targeted molecules into polymer networks was confirmed by the presence of key spectral features in all spectra. The P1 spectrum exhibits the characteristic C=O carbonyl band at 1723 cm^{-1}, along with P=O and P–O–C stretching vibrations observed between 1000 and 1250 cm^{-1}.[36] Subsequently, the intensity of the C=O band at 1723 cm^{-1} increases in P2, indicating the successful incorporation of the POEGMEMA block. The presence of the C=O band of the aldehyde group at 1686 cm^{-1}, the aromatic C=C stretching vibrations of the benzene ring of FPMA at 1509 and 1600 cm^{-1}, and the H–CO stretching vibrations at 2869 and 2730 cm^{-1} in the P3 spectrum all confirm that the targeted monomer unit has been successfully incorporated into the polymer network.[37] Following the conjugation of Dox to P4, the intensity of the aldehyde band at 1600 cm^{-1} decreases in the P4-Dox spectrum. The broad absorption band between 3100 and 3600 cm^{-1}, which is attributed to the aromatic OH groups of Dox, also confirms successful conjugation.

3.1. Micelle formation

A pH responsive polymeric nanomicelle system containing Dox and/or Aln was simply prepared by nanoprecipitation methods in aqueous solution. From DLS measurements, it was possible to conclude that micelle size (M0) without drugs increased from about 48.9 ± 7.42 to around 100.00 ± 6.34, 97.70 ± 4.39, and 89.86 ± 4.77 for M1 (Dox-loaded), M2 (Aln-loaded), and M3 (dual drug-loaded), respectively (Table 2, Figure 2(a)). DLS result is in agreement with TEM images, demonstrating the micelles with uniform morphology and size diameters ranging between 85 and 95 nm (Figure 2(a)). The presence of bisphosphonic acid groups on the shells of the micelles gives them a negative charge, as indicated by zeta (ζ) potential values of −15.22 ± 1.32, −8.79 ± 0.17, −9.58 ± 0.39, and −9.27 ± 1.37 mV, as determined by DLS measurements for M0, M1, M_2, and M_3, respectively. Notably, the close similarity in micelle sizes across the formulations (Table 2) is advantageous, as it facilitates reliable *in vitro* comparisons of their biological performance under consistent size-dependent conditions. Additionally, size and morphology of M1 and M3 micelles were characterized by TEM analysis (Figure 2(b)). The average particle size values obtained from the TEM analysis of M1 and M3 were found to be 85.3 ± 13.9 and 120.8 ± 12.6, respectively, and the micelles appeared to be spherical-like in shape.

Dox amounts of the micelles were also determined by UV–vis spectroscopy by using the calibration curve created with known Dox amounts, with M1 and M3 maximum absorbance values (Figure 2(c)) to achieve this, the micelles were treated with a methanol solution to disassemble them. The Dox amounts of M1 and M3 were found as 20.7 μg/mL and 22.4 μg/mL. UV–vis analysis was also used to determine the Aln loading capacity (LC) and encapsulation efficiencies (EE). The Aln LC of M2 and M3 were calculated to be 13.7.0% and 12.8%, based on the calibration curve created using known quantities of the Aln–$FeCl_3$ complex (Figure S3), with maximum absorbance values of $FeCl_3$ and Aln at around 280 nm for M_2 and M_3. Also, according to the results EE were calculated to be 68.8% and 64.4% for M2 and M3, respectively (Figure 2(d)).

3.2. Drug release

To evaluate the pH-responsive drug release behavior, dialysis experiments were conducted containing Dox-loaded micelles (M1 and M3) immersed in PBS at two different pH values; 7.4 (physiological) and 5.5 (tumor-mimicking acidic conditions). At pH 7.4, the cumulative Dox release over 24 h was limited to 28% for M1 and 33% for M3. After 80 h, the release slightly increased to 34% and 38%, respectively, indicating minimal drug release under physiological conditions. These results suggest that the imine linkage between Dox and the FPMA units remained largely intact at neutral pH, consistent with the known stability of imine bonds under such conditions (Figure 2(e)). In contrast, at pH 5.5—mimicking the acidic tumor microenvironment—the imine bonds underwent accelerated hydrolysis, leading to a markedly faster release of Dox. Within the first 24 h, the cumulative release reached 71% and 67% for M1 and M3, respectively. By the end of 80 h, nearly complete drug release was achieved, with 93–98% of the conjugated Dox released under acidic conditions. These findings confirm the pH-responsive nature of the micellar system, making it a promising platform for selective drug release in tumor environments. Drug release mechanisms based on pH-sensitive bonds have been widely explored in recent studies. Ye et al. developed a micelle-based dual drug delivery system for bone cancer treatment, incorporating the bone-targeting agent alendronate and the chemotherapeutic drug Dox within a polymeric backbone.[38] The nanosystem demonstrated desirable physicochemical properties, effective *in vitro* cytotoxicity, and significant *in vivo* antitumor activity. Importantly, drug release from the micelles was pH-responsive, with reduced systemic toxicity compared to the free drug. Similarly, Abdelmoneem et al. designed Aln-functionalized porous silicon nanoparticles that exhibited sustained and pH-dependent Dox release. Their system showed significantly enhanced drug release under acidic conditions, supporting the rationale for using pH-sensitive nanocarriers in OS therapy and highlighting the role of the tumor microenvironment in triggering intracellular drug release.[39] Likewise, Zhou et al. reported imine-linked polymeric micelles that released Dox rapidly and selectively under mildly acidic conditions. These

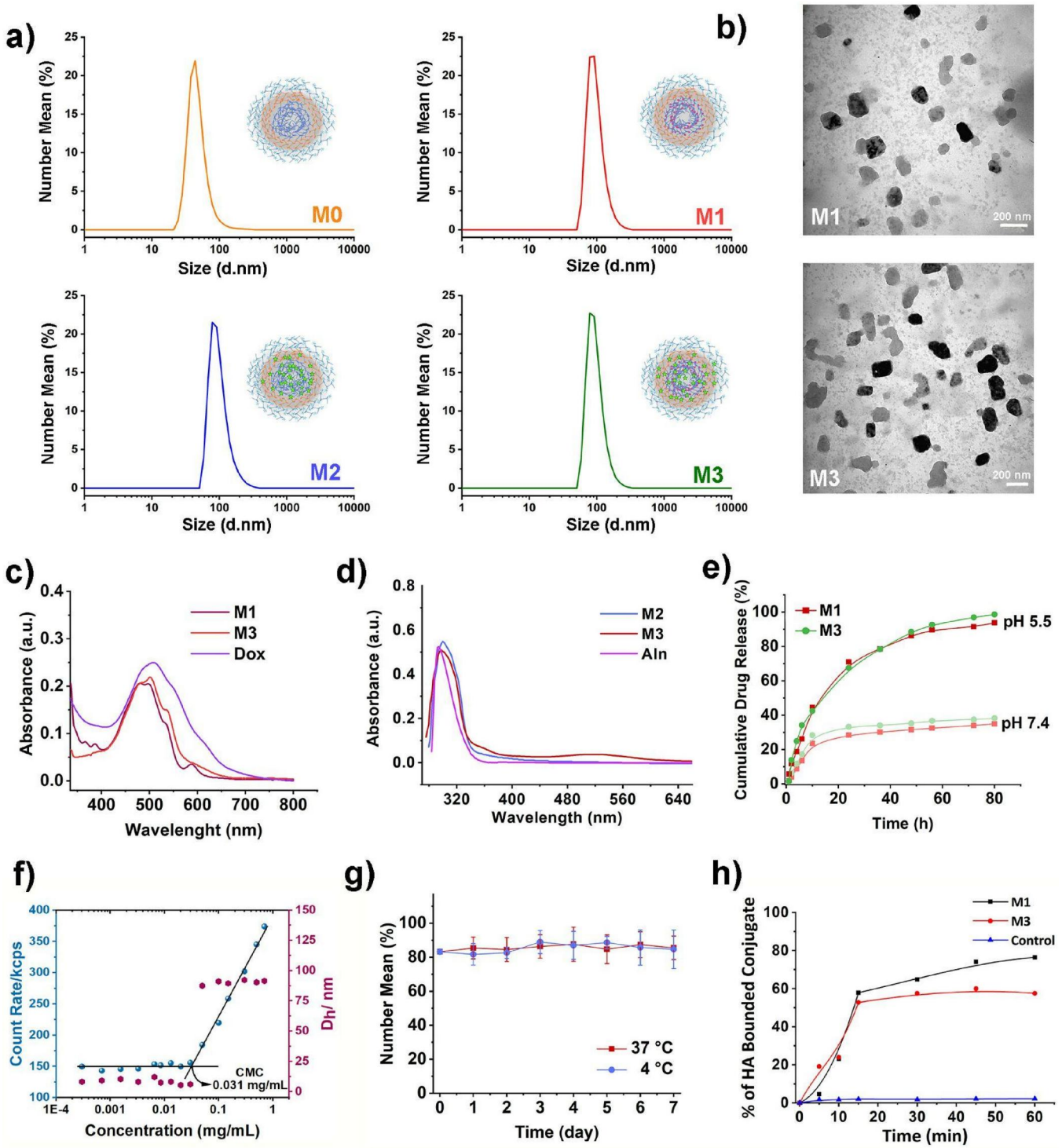

Figure 2. a) Size distribution of micelle formulations determined by DLS analysis, b) TEM images of M1 and M3, scale bar: 200 nm c) UV–vis spectra of 45 μg/mL of M1, M3 and 12 μg/mL Dox, d) UV-vis spectra of $FeCl_3$ derivatives of 200 μg/mL M2, M3 and 100 μg/mL Aln. e) Cumulative drug release profile of M1 and M3 at pH 7.4 and pH 5.5, f) Critical micelle concentration, and g) Serum stability of M3 determined by DLS analysis, h) Bone binding efficiency of M1 and M3 micelles.

Table 1. Polymerization conditions and molecular weight characteristics of amphiphilic triblock copolymer and its precursor polymers.

Code	Polymer	[M]:[RAFT]:[I]	Time (h)	Conv.a (%)	$M_{n,GPC}$ (kDa)	Đ	$M_{n,NMR}$ (kDa)
P1	P(BPMA)	[50]:[1]:[0.10]	8	46	13.98[b]	1.08	11.10
P2	P(BPMA-*b*-OEGMEMA)	[120]:[1]:[0.12]	14.5	83	16.90[b]	1.10	41.10
P3	P(BPMA-*b*-OEGMEMA-*b*-FPMA)	[120]:[1]:[0.15]	16	86	53.80[c]	1.23	65.20
P4	P(BPMA-*b*-OEGMEMA-*b*-FPMA)-hyd	–	–		50.10[c]	1.28	61.50

[a]Conversion was determined by ^{1}H NMR spectroscopy.[35] Number-average molecular weight (Mn) and polydispersity index (Đ) were obtained from [b]THF GPC and [c]DMF GPC-MALS analyses, respectively.

Table 2. Physicochemical characterization of micelles with their respective size, polydispersity index (Đ), and zeta potential (ζ-potential) values.

Code	Micelles	Size (nm)	Đ	ζ-potential (mV)
M0	P4	48.9 ± 7.42	0.384	−15.22 ± 1.32
M1	P4-Dox	100.00 ± 6.34	0.107	−8.79 ± 0.17
M2	P4-Aln	97.70 ± 4.39	0.330	−9.58 ± 0.39
M3	P4-Dox-Aln	89.86 ± 4.77	0.175	−9.27 ± 1.37

micelles remained stable at physiological pH but enabled efficient intracellular drug release in tumor-like environments, emphasizing the potential of dynamic imine chemistry as a pH-responsive trigger.[40]

3.3. Critical micelle concentration (CMC)

Determining the CMC of micelles, a value that indicates micelle stability, is important in biological applications. Figure 2(f) shows the relationship between the concentration of the M3 micelle and its DLS intensity. Samples of M3 were prepared at concentrations ranging from 4.0×10^{-4} mg/mL to 0.8 mg/mL. The intensity of scattered light, expressed in kilocounts per second (kcps), was recorded for each concentration. The CMC was identified as the intersection point of the extrapolated linear regions corresponding to low and high concentration ranges on the kcps versus concentration plot. The slope changes above the critical concentration, resulting in a CMC value of 31 µg/mL. Furthermore, the micelle size mean is 90.4 ± 1.7 above the CMC, but after CMC, the average size values decrease due to the disruption of micelle integrity. The determined CMC value indicates that M3 can maintain its stability after dilution in biological applications.

3.4. In vitro serum stability of dual drug-loaded polymeric micelles

Polymeric micelles are expected to maintain their structural integrity in the bloodstream in order to ensure the efficient delivery of drugs. To evaluate the *in vitro* serum stability of the dual drug-loaded M3 micelle formulation, a time-dependent stability study was conducted under physiologically relevant conditions. It is known that micelles interact with serum components, which can lead to aggregation or disassembly due to protein adsorption and significantly impact the performance of the delivery system.[41] To this end, M3 micelles were incubated in DMEM supplemented with 10% FBS at two different temperatures: 4 °C and 37 °C. The initial hydrodynamic diameter of M3 at 37 °C was measured as 83.24 ± 2.88 nm using DLS. Over the course of seven days, only a minor increase in particle size was observed: 2.91 nm at 37 °C and 3.46 nm at 4 °C (Figure 2(g)). These results indicate that M3 micelles demonstrate high colloidal stability in the presence of serum proteins, with minimal variation in particle size over time. The slightly greater stability observed at 37 °C compared to 4 °C may be due to temperature-dependent interactions between the micelles and serum components. Notably, the negligible size changes indicate an absence of significant protein adsorption or micelle disruption under both conditions. Dual drug-loaded M3 micelles demonstrated robust physicochemical stability in serum-containing media, supporting their potential as biocompatible, stable nanocarriers for systemic drug delivery applications.

3.5. Bone binding assay

The selectivity of the nanocarriers toward target cells was evaluated using a HA binding assay (Figure 2(h)). The extent of nanocarrier binding to HA was monitored over 60 min by measuring the UV absorbance of Dox, which had been conjugated to the polymer. This allowed the amount of HA-bound versus unbound nanocarriers to be quantified. As a control, Dox was conjugated to the unhydrolysed P3 polymer, which formed less than 2% HA conjugate after 60 min, demonstrating minimal nonspecific binding in the absence of bisphosphonic acid groups. By contrast, M1 and M3 micelles exhibited significant HA affinity, with 76.4% and 57.6% HA conjugation respectively at the end of the incubation period. The slightly reduced HA binding observed for M3 is likely due to competitive interactions between Aln molecules within the M3 micelles and the HA-binding linker groups present on the nanocarrier surface, which may partially hinder conjugate formation.[42] These findings confirm that the bisphosphonic acid moieties on the nanocarrier surface play a critical role in HA targeting by enhancing selective binding to bone-like mineral environments that are relevant for OS therapy.[7]

3.6. In vitro assays

The cytotoxic effect of mono or dual drug-loaded micelles and free drugs was evaluated in the SAOS-2 OS cell line and as a healthy control HUVEC cell line. The effect of the micelles was evaluated by MTT assay after 24 h of incubation. Compared to HUVEC, SAOS-2 cells were more sensitive to M3, while there were no cytotoxicity effects observed in all cells treated with M0 without drugs. Free Dox and free Aln had IC_{50} values of 46.85 ± 4.22 and 66.84 ± 3.37 µg/mL for HUVEC, and 39.46 ± 5.08 and 54.09 ± 6.81 µg/mL for SAOS-2, respectively (Table S1). The IC_{50} value of Dox-loaded micelle M1 was found to be 212.1 µg/mL for HUVEC, while it was 21.9 µg/mL for SAOS-2. Both Aln and Dox dually loaded micelles M3 had the lowest IC_{50} values for SAOS-2 cells found to be 13.1 µg/mL. MTT assay results show that bone-targeted micelle formulations have greater cytotoxic effects on SAOS-2 OS cell line compared to HUVEC cell line (Figure 3).

When the selectivity indices (TD_{50}/ED_{50}) of the formulations were evaluated, it was found that the free drugs and blank micelle formulation showed no significant selectivity between the two cell lines (Table S1). By contrast, drug-loaded micelles, particularly M1 (Dox-loaded) and M3(dual drug-loaded), demonstrated markedly higher selectivity indices, indicating enhanced preferential cytotoxicity toward cancer cells.[43] The combination index (CI) of the M3 micelle was calculated using the IC_{50} values of the M3, M2,

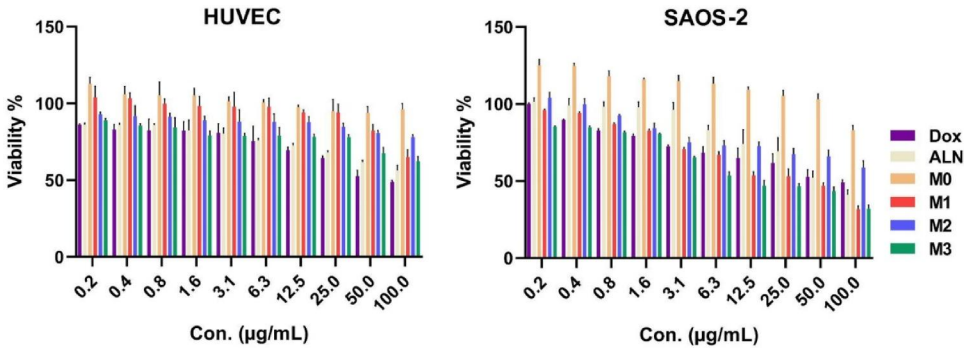

Figure 3. Cytotoxicity evaluation of free drugs and micelle formulations on HUVEC and SAOS-2 cells. Cell viability was assessed after 24 h treatment with ten different concentrations of M0, M1, M2, M3, free Dox and free Aln. Viability was determined by MTT assay and is expressed as a percentage relative to untreated controls (mean ± SD). ($n = 3$ independent experiments). Con.: concentration.

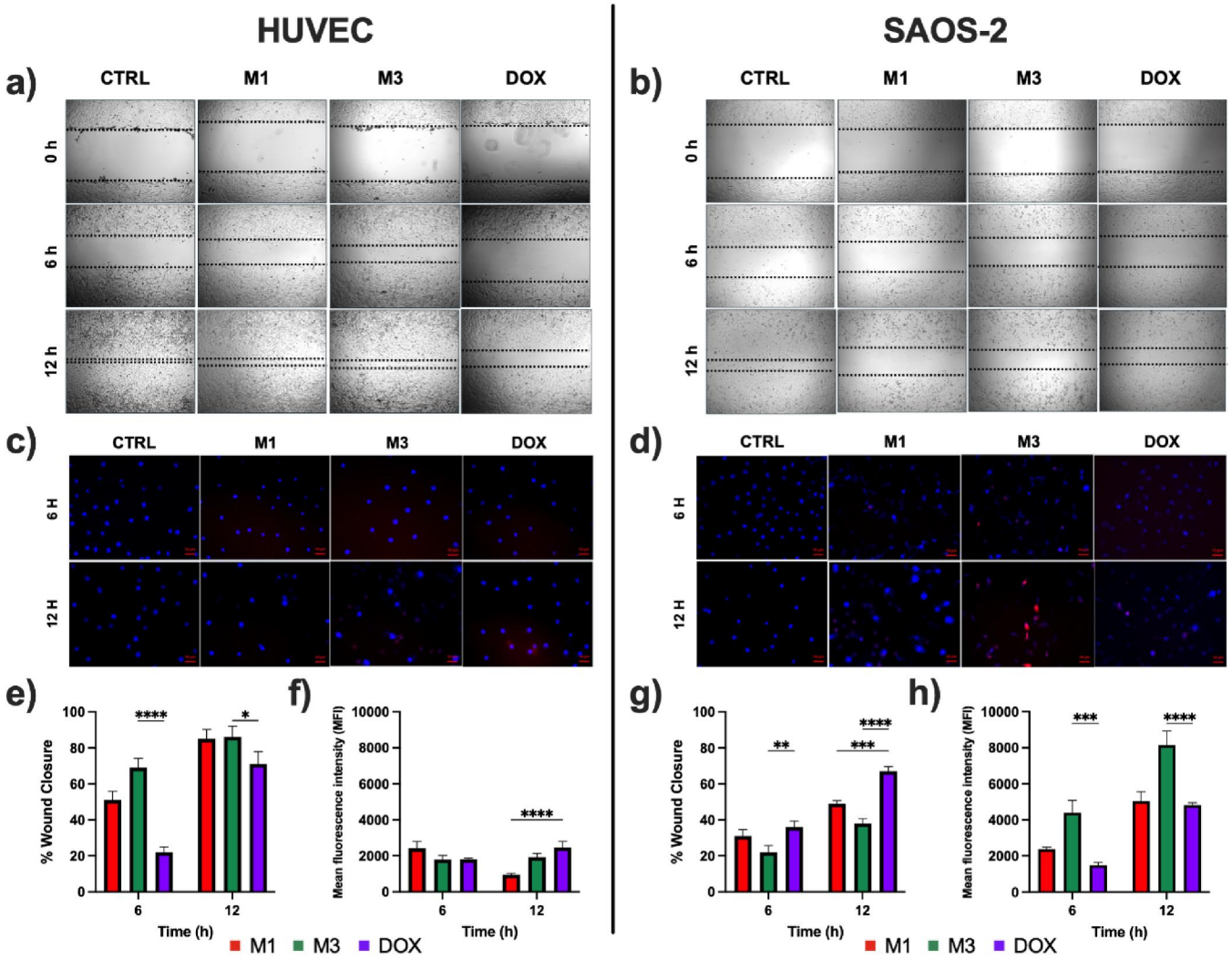

Figure 4. Evaluation of cell migration and cellular uptake following treatment with M1, M3, and Dox. (a, b) Representative phase-contrast images of scratch assays in HUVEC (a) and SAOS-2 (b) monolayers at 0 h, 6 h, and 12 h following treatment with M1, M3, Dox or untreated control (CTRL). The dotted lines indicate the wound margins. (c, d) Fluorescence microscopy images of HUVEC (c) and SAOS-2 (d) cells stained at 6 h and 12 h post-treatment (Nuclei: DAPI, blue. Intracellular Dox fluorescence: red). (e, g) Quantitative analysis of wound closure (%) for HUVEC (e) and SAOS-2 (g) cells, confirming that M1 and M3 did not significantly affect migration in normal endothelial cells but restrict migration in osteosarcoma cells. (f, h) Quantification of mean fluorescence intensity (MFI) in HUVEC (f) and SAOS-2 (h) cells, showing preferential uptake of M3 and Dox in osteosarcoma cells, while uptake remained minimal in HUVECs. Data represent mean ± SD ($n = 3$ independent experiments). Statistical analysis was performed using one-way ANOVA with Tukey's post hoc test (*$p < 0.05$, **$p < 0.01$, ***$p < 0.001$, ****$p < 0.0001$).

and M1 micelles. Based on the IC_{50} data obtained from SAOS-2 cells, the CI value for M3 was found to be less than 1, suggesting that the dual-drug-loaded micelle exhibits a synergistic cytotoxic effect.[44]

To assess the effects of the M1, M3, and free Dox on cell migration, scratch assay was performed on both cell lines (Figure 4(a and b)). In HUVEC cells, M1 and M3 treatments did not inhibit cell proliferation or migration,

indicating that the Dox-loaded nanocarriers did not exert a toxic effect on healthy cells and demonstrated better biocompatibility. M1 and M3 treatments caused wound closure compared to free Dox, with M3 demonstrating the highest closure rate at both 6 h and 12 h ($p < 0.0001$ and $p < 0.05$, respectively) (Figure 4(e)). In SAOS-2 cells, both M1 and M3 treatments significantly suppressed wound closure compared to control. In contrast to free Dox, M3 significantly suppressed migration of cells at 6 h and 12 h ($p < 0.001$ and $p < 0.0001$, respectively), highlighting its potent cytotoxicity (Figure 4(g)). It was also demonstrated that M3 exhibited stronger inhibition than M1, indicating the synergistic and targeted effects of alendronate and Dox in reducing OS cell migration. These results highlight the potential of M3 to selectively suppress tumor cell migration without compromising the viability of normal cells, aligning with the intended bone-targeted antitumor strategy.

To evaluate the uptake efficiency of the nanocarriers, fluorescence microscopy was performed using the intrinsic fluorescence of Dox. In HUVEC cells (Figure 4(c)), relatively low levels of fluorescence intensities were observed in M1, M3, and Dox groups at both 6 h and 12 h, as confirmed by quantitative MFI data (Figure 4(f)). M1 exhibited significantly lower uptake at 12 h compared to the M3 and Dox, suggesting minimal interaction or internalization of the Dox-loaded nanocarriers by HUVEC. This limited uptake is favorable, indicating a reduced risk of off-target toxicity in normal cells. In contrast, SAOS-2 OS cells demonstrated higher fluorescence intensities, especially in the M3-treated group (Figure 4(d)). Quantitative analysis revealed that M3 significantly enhanced cellular uptake at both 6 h and 12 h compared to M1 and free Dox ($p < 0.001$ and $p < 0.0001$, respectively) (Figure 4(h)). These results suggested that M3 provides superior internalization in OS cells, due to Aln's bone-targeting properties and its affinity for HA-enriched tumor environments.[45] The increased uptake correlates with the stronger inhibitory effects on SAOS-2 migration observed in the scratch assay. This further supports the validity of M3 as a targeted drug delivery strategy with selective cytotoxicity toward OS cells.

4. Conclusions

This study successfully developed a bone-targeted, pH-sensitive, triblock copolymer-based nanocarrier system for the dual delivery of Dox and Aln, to improve therapeutic outcomes in the treatment of OS. All the nanocarriers exhibited similar sizes and surface charges according to DLS and TEM analyses. This study demonstrated that polymeric nanocarriers can be densely conjugated with Dox, resulting in the efficient and sustained release of therapeutic drugs. The synthesized micelles exhibited favorable physicochemical properties, including a nanoscale size, monodispersity and colloidal stability, as confirmed by DLS analysis. Of the various formulations, dual-loaded micelles (M3) exhibited the most potent anti-cancer activity against SAOS-2 cells, demonstrating significantly enhanced cytotoxicity while maintaining excellent biocompatibility with non-cancerous HUVEC cells. Furthermore, fluorescence imaging confirmed the efficient uptake of the micelles by OS cells, thus validating the bone-targeting capability of the designed system. These findings highlight the potential of this smart nanocarrier platform for selectively targeting bone tissue, achieving site-specific drug delivery, and enhancing therapeutic outcomes synergistically in the treatment of OS, while reducing off-target effects and systemic toxicity. These findings suggest that the proposed dual-drug nanocarrier system may serve as a promising candidate for future preclinical studies in bone cancer therapy.

Acknowledgments

The authors thank pharmaceutical companies DEVA and KOCAK PHARMA for the donation of therapeutic drug alendronate and doxorubicin. We sincerely thank Sinem Atasoy for her valuable contribution in creating the bone illustration.

Disclosure statement

No potential conflict of interest was reported by the author(s).

Funding

This work was financially supported by Bezmialem Vakif University (Scientific Research Project Number: E11.2019/1 and 20230620).

ORCID

Isinsu Mutlu http://orcid.org/0009-0007-0358-1727
Tugba Gencoglu-Katmerlikaya http://orcid.org/0000-0003-3989-8711
Sezen Atasoy http://orcid.org/0000-0001-5063-5053
Aydan Dag http://orcid.org/0000-0002-1552-8030

References

[1] Ritter, J.; Bielack, S. S. Osteosarcoma. *Ann. Oncol.* **2010**, *21 Suppl 7*, vii320–5. DOI: 10.1093/annonc/mdq276.
[2] Kansara, M.; Teng, M. W.; Smyth, M. J.; Thomas, D. M. Translational Biology of Osteosarcoma. *Nat. Rev. Cancer* **2014**, *14*, 722–735. DOI: 10.1038/nrc3838.
[3] Chen, Y.; Cao, J.; Zhang, N.; Yang, B.; He, Q.; Shao, X.; Ying, M. Advances in Differentiation Therapy for Osteosarcoma. *Drug Discov. Today.* **2020**, *25*, 497–504. DOI: 10.1016/j.drudis.2019.08.010.
[4] Gill, J.; Gorlick, R. Advancing Therapy for Osteosarcoma. *Nat. Rev. Clin. Oncol.* **2021**, *18*, 609–624. DOI: 10.1038/s41571-021-00519-8.
[5] Porras, A. G.; Holland, S. D.; Gertz, B. J. Pharmacokinetics of Alendronate. *Clin. Pharmacokinet.* **1999**, *36*, 315–328. DOI: 10.2165/00003088-199936050-00002.
[6] Ananchenko, G.; Novakovic, J.; Tikhomirova, A. Alendronate Sodium. *Prof. Drug Subst. Excip. Relat. Methodol.* **2013**, *38*, 1–33. DOI: 10.1016/B978-0-12-407691-4.00001-0.
[7] Huang, H.; Asghar, S.; Lin, L.; Chen, S.; Yuan, C.; Sang, M.; Xiao, Y. Design and Evaluation of a Multi-Responsive Dual-Modality Bone-Targeted Drug Delivery Vehicle for the Treatment of Osteosarcoma. *Int. J. Pharm.* **2025**, *671*, 125191. DOI: 10.1016/j.ijpharm.2025.125191.
[8] Sun, K.; Yuan, L.; Chen, S.; Sun, Y.; Wei, D. Alendronate Pt(IV) Prodrug Amphiphile for Enhanced Chemotherapy Targeting and Bone Destruction Inhibition in Osteosarcoma.

Adv. Healthc. Mater. **2024**, *13*, e2302746. DOI: 10.1002/adhm.202302746.

[9] Xie, D.; Wang, Z.; Li, J.; Guo, D. A.; Lu, A.; Liang, C. Targeted Delivery of Chemotherapeutic Agents for Osteosarcoma Treatment. *Front. Oncol.* **2022**, *12*, 843345. DOI: 10.3389/fonc.2022.843345.

[10] Jia, S.; Chen, Y.; Zhuo, C.; Hu, M.; Zhang, C.; Cai, H.; Li, X.; Chen, H.; Yu, X. Aptamer-Modified Melittin Micelles Efficiently Inhibit Osteosarcoma Deterioration by Inducing Immunogenic Cell Death. *Coll. Surf. B Biointerf.* **2025**, *249*, 114512. DOI: 10.1016/j.colsurfb.2025.114512.

[11] Liu, Y.; Jiang, Z.; Tong, S.; Sun, Y.; Zhang, Y.; Zhang, J.; Zhao, D.; Su, Y.; Ding, J.; Chen, X. Acidity-Triggered Transformable Polypeptide Self-Assembly to Initiate Tumor-Specific Biomineralization. *Adv. Mater.* **2023**, *35*, e2203291.

[12] Sha, Z.; Yang, S.; Fu, L.; Geng, M.; Gu, J.; Liu, X.; Li, S.; Zhou, X.; He, C. Manganese-Doped Gold Core Mesoporous Silica Particles as a Nanoplatform for Dual-Modality Imaging and Chemo-Chemodynamic Combination Osteosarcoma Therapy. *Nanoscale* **2021**, *13*, 5077–5093. DOI: 10.1039/d0nr09220g.

[13] Wu, Y.; Sun, B.; Tang, Y.; Shen, A.; Lin, Y.; Zhao, X.; Li, J.; Monteiro, M. J.; Gu, W. Bone Targeted Nano-Drug and Nano-Delivery. *Bone Res.* **2024**, *12*, 51. DOI: 10.1038/s41413-024-00356-2.

[14] Chen, Y.; Wu, X.; Li, J.; Jiang, Y.; Xu, K.; Su, J. Bone-Targeted Nanoparticle Drug Delivery System: An Emerging Strategy for Bone-Related Disease. *Front. Pharmacol.* **2022**, *13*, 909408. DOI: 10.3389/fphar.2022.909408.

[15] Sun, X.; Lin, Y.; Zhong, X.; Fan, C.; Liu, Z.; Chen, X.; Luo, Z.; Wu, J.; Tima, S.; Zhang, Z.; et al. Alendronate-Functionalized Polymeric Micelles Target Icaritin to Bone for Mitigating Osteoporosis in a Rat Model. *J. Control. Release* **2024**, *376*, 37–51. DOI: 10.1016/j.jconrel.2024.10.002.

[16] Karacivi, M.; Sumer Bolu, B.; Sanyal, R. Targeting to the Bone: Alendronate-Directed Combretastatin A-4 Bearing Antiangiogenic Polymer-Drug Conjugates. *Mol. Pharm.* **2017**, *14*, 1373–1383. DOI: 10.1021/acs.molpharmaceut.6b01173.

[17] Guven, M. N.; Demirci, G.; Altuncu, S.; Gulyuz, U.; Okay, O.; Yagci Acar, H.; Avci, D. Alendronate-Functionalized Poly(Amido Amine) Cryogels of High-Toughness for Biomedical Applications. *Polymer. (Guildf)* **2020**, *190*, 122248. DOI: 10.1016/j.polymer.2020.122248.

[18] Young, R. N.; Grynpas, M. D. Targeting Therapeutics to Bone by Conjugation with Bisphosphonates. *Curr. Opin. Pharmacol.* **2018**, *40*, 87–94. DOI: 10.1016/j.coph.2018.03.010.

[19] Cetin Ersen, B.; Goncu, B.; Dag, A.; Birlik Demirel, G. GLUT-Targeting Phototherapeutic Nanoparticles for Synergistic Triple Combination Cancer Therapy. *ACS Appl. Mater. Interfaces.* **2023**, *15*, 9080–9098. DOI: 10.1021/acsami.2c21180.

[20] Xing, Y.; Qiu, L.; Liu, D.; Dai, S.; Sheu, C. L. The Role of Smart Polymeric Biomaterials in Bone Regeneration: A Review. *Front. Bioeng. Biotechnol.* **2023**, *11*, 1240861. DOI: 10.3389/fbioe.2023.1240861.

[21] Li, M.; Yu, B.; Wang, S.; Zhou, F.; Cui, J.; Su, J. Microenvironment-Responsive Nanocarriers for Targeted Bone Disease Therapy. *Nano Today* **2023**, *50*, 101838. DOI: 10.1016/j.nantod.2023.101838.

[22] Atasoy, S.; Gencoglu Katmerlikaya, T.; Sancakli, B.; Dag, A. Remote-Controlled Release of Therapeutics from Multifunctional Glycoplexes Inhibit Melanoma Cells. *Eur. Polym. J.* **2025**, *226*, 113726. DOI: 10.1016/j.eurpolymj.2025.113726.

[23] Khine, Y. Y.; Jiang, Y.; Dag, A.; Lu, H.; Stenzel, M. H. Dual-Responsive pH and Temperature Sensitive Nanoparticles Based on Methacrylic Acid and Di(Ethylene Glycol) Methyl Ether Methacrylate for the Triggered Release of Drugs. *Macromol. Biosci.* **2015**, *15*, 1091–1104. DOI: 10.1002/mabi.201500057.

[24] Dag, A.; Cakilkaya, E.; Omurtag Ozgen, P. S.; Atasoy, S.; Yigit Erdem, G.; Cetin, B.; Çavuş Kokuroğlu, A.; Gürek, A. G. Phthalocyanine-Conjugated Glyconanoparticles for Chemo-Photodynamic Combination Therapy. *Biomacromolecules* **2021**, *22*, 1555–1567. DOI: 10.1021/acs.biomac.0c01811.

[25] Hu, N.; Johnson, L. M.; Pothayee, N.; Pothayee, N.; Lin, Y.; Davis, R. M.; Riffle, J. S. Synthesis of Ammonium Bisphosphonate Monomers and Polymers. *Polymer. (Guildf)* **2013**, *54*, 3188–3197. DOI: 10.1016/j.polymer.2013.04.032.

[26] Kuljanin, J.; Janković, I.; Nedeljković, J.; Prstojević, D.; Marinković, V. Spectrophotometric Determination of Alendronate in Pharmaceutical Formulations via Complex Formation with Fe(III) Ions. *J. Pharm. Biomed. Anal.* **2002**, *28*, 1215–1220. DOI: 10.1016/s0731-7085(02)00021-3.

[27] Degrand, L.; Garcia, R.; Crouvisier Urion, K.; Guiga, W. Dynamic Light Scattering for the Determination of Linoleic Acid Critical Micelle Concentration. Effect of pH, Ionic Strength, and Ethanol. *J. Mol. Liq.* **2023**, *388*, 122670. DOI: 10.1016/j.molliq.2023.122670.

[28] Liu, Z.; Chen, X.; Jin, Q.; Li, M.; Zhu, S.; Zhang, Y.; Zhi, D.; Zhao, Y.; Li, L.; Zhang, S. Dual Functionalized Hyaluronic Acid Micelles Loading Paclitaxel for the Therapy of Breast Cancer. *Front. Bioeng. Biotechnol.* **2023**, *11*, 1230585. DOI: 10.3389/fbioe.2023.1230585.

[29] Chen, H.; Li, G.; Chi, H.; Wang, D.; Tu, C.; Pan, L.; Zhu, L.; Qiu, F.; Guo, F.; Zhu, X. Alendronate-Conjugated Amphiphilic Hyperbranched Polymer Based on Boltorn H40 and Poly(Ethylene Glycol) for Bone-Targeted Drug Delivery. *Bioconjug. Chem.* **2012**, *23*, 1915–1924. DOI: 10.1021/bc3003088.

[30] Yigit Erdem, G.; Goncu, B.; Atasoy, S.; Yildiz Uysal, A.; Dag, S.; Dag, A. Multifunctional Theranostic Glyconanoprobes for Synergistic Eradication of Breast Cancer. *J. Mater. Chem. B* **2025**, *13*, 2150–2166. DOI: 10.1039/d4tb02550d.

[31] Sevgi, E.; Dag, A.; Kızılarslan-Hançer, Ç.; Atasoy, S.; Kurt, B. Z.; Aksakal, Ö. Evaluation of Cytotoxic and Antioxidant Potential of Dittrichia Viscosa (L.) Greuter Used in Traditional Medicine. *J. Ethnopharmacol.* **2021**, *276*, 114211. DOI: 10.1016/j.jep.2021.114211.

[32] Omurtag Ozgen, P. S.; Atasoy, S.; Zengin Kurt, B.; Durmus, Z.; Yigit, G.; Dag, A. Glycopolymer Decorated Multiwalled Carbon Nanotubes for Dual Targeted Breast Cancer Therapy. *J. Mater. Chem. B* **2020**, *8*, 3123–3137. DOI: 10.1039/c9tb02711d.

[33] Dag, A.; Omurtag Ozgen, P. S.; Atasoy, S. Glyconanoparticles for Targeted Tumor Therapy of Platinum Anticancer Drug. *Biomacromolecules* **2019**, *20*, 2962–2972. DOI: 10.1021/acs.biomac.9b00528.

[34] Gunaydin-Akyildiz, A.; Yanikoglu, R. S.; Gulec, M.; Alim-Toraman, G. O.; Kuran, E. D.; Atasoy, S.; Olgun, A.; Topcu, G. Emodin and Aloe-Emodin, Two Potential Molecules in Regulating Cell Migration of Skin Cells through the MAP Kinase Pathway and Affecting Caenorhabditis elegans Thermotolerance. *BMC Mol. Cell Biol.* **2023**, *24*, 23. DOI: 10.1186/s12860-023-00486-1.

[35] Izunobi, J. U.; Higginbotham, C. L. Polymer Molecular Weight Analysis by 1H NMR Spectroscopy. *J. Chem. Educ.* **2011**, *88*, 1098–1104. DOI: 10.1021/ed100461v.

[36] Thomas, L. C.; Chittenden, R. A. Characteristic Infrared Absorption Frequencies of Organophosphorus Compounds—II. P—O—(X) bonds. *Spectrochim. Acta* **1964**, *20*, 489–502. DOI: 10.1016/0371-1951(64)80044-8.

[37] Zhai, Y.; Zhou, X.; Zhang, Z.; Zhang, L.; Wang, D.; Wang, X.; Sun, W. Design, Synthesis, and Characterization of Schiff Base Bond-Linked pH-Responsive Doxorubicin Prodrug Based on Functionalized mPEG-PCL for Targeted Cancer Therapy. *Polymers. (Basel)* **2018**, *10*, 1127. DOI: 10.3390/polym10101127.

[38] Ye, W. L.; Zhao, Y. P.; Li, H. Q.; Na, R.; Li, F.; Mei, Q. B.; Zhao, M. G.; Zhou, S. Y. Doxorubicin-Poly (Ethylene Glycol)-Alendronate Self-Assembled Micelles for Targeted Therapy of Bone Metastatic Cancer. *Sci. Rep.* **2015**, *5*, 14614. DOI: 10.1038/srep14614.

[39] M, A. A.; Esser, L.; Wojnilowicz, M.; Voelcker, N. H. Surface-Engineered Porous Silicon Nanoparticles for Targeted Osteosarcoma Therapy. *Biomacromolecules* **2025**, *26*, 5020–5031. DOI: 10.1021/acs.biomac.5c00409.

[40] Tao, Y.; Liu, S.; Zhang, Y.; Chi, Z.; Xu, J. A pH-Responsive Polymer Based on Dynamic Imine Bonds as a Drug Delivery Material with Pseudo Target Release Behavior. *Polym. Chem.* **2018**, *9*, 878–884. DOI: 10.1039/C7PY02108A.

[41] Lu, J.; Owen, S. C.; Shoichet, M. S. Stability of Self-Assembled Polymeric Micelles in Serum. *Macromolecules* **2011**, *44*, 6002–6008. DOI: 10.1021/ma200675w.

[42] Leu, C. T.; Luegmayr, E.; Freedman, L. P.; Rodan, G. A.; Reszka, A. A. Relative Binding Affinities of Bisphosphonates for Human Bone and Relationship to Antiresorptive Efficacy. *Bone* **2006**, *38*, 628–636. DOI: 10.1016/j.bone.2005.07.023.

[43] Badmus, J. A.; Ekpo, O. E.; Hussein, A. A.; Meyer, M.; Hiss, D. C. Cytotoxic and Cell Cycle Arrest Properties of Two Steroidal Alkaloids Isolated from Holarrhena Floribunda (G. Don) T. Durand & Schinz Leaves. *BMC Complement. Altern. Med.* **2019**, *19*, 112. DOI: 10.1186/s12906-019-2521-9.

[44] Bhatnagar, P.; Bansal, R.; Vishwakarma, V. K.; Yadav, H. N.; Dinda, A. K.; Gupta, Y. K. pH Responsive Dextran Nanoparticles Loaded with Doxorubicin and RITA against Cancer Cells: Synergistic Inhibitory Effects. *J. Nanopart. Res.* **2024**, *26*, 135. DOI: 10.1007/s11051-024-06032-0.

[45] Damasco, J. A.; Yu, G.; Kumar, A.; Perez, J.; Lirag, R. C. M.; Whitley, E. M.; Lin, S. H.; Melancon, M. P. Alendronate Conjugate for Targeted Delivery to Bone-Forming Prostate Cancer. *Talanta* **2023**, *256*, 124308. DOI: 10.1016/j.talanta.2023.124308.